Solvent electrospinning amorphous solid dispersions with high Itraconazole, Celecoxib, Mebendazole and Fenofibrate drug loading and release potential

Jana Becelaere[a], Olmo Frateur[a], Ella Schoolaert[a], Valérie Vanhoorne[b], Dagmar R. D'hooge[a], Chris Vervaet[b,*], Richard Hoogenboom[c,*], Karen De Clerck[a,*]

[a]Ghent University, Department of Materials, Textiles and Chemical Engineering, Faculty of Engineering and Architecture, Technologiepark 70A, B-9052 Ghent, Belgium - +32 (0)9 264 57 40 – karen.declerck@ugent.be
[b]Ghent University, Laboratory of Pharmaceutical Technology, Department of Pharmaceutics, Faculty of Pharmaceutical Sciences, Ottergemsesteenweg 460, B-9000 Ghent, Belgium - +32 (0)9 264 44 82 – chris.vervaet@ugent.be
[c]Ghent University, Supramolecular Chemistry Group, Centre of Macromolecular Chemistry (CMaC), Department of Organic and Macromolecular Chemistry, Faculty of Sciences, Krijgslaan 281 - S4, B-9000 Ghent, Belgium - +32 (0)9 264 80 69 –richard.hoogenboom@ugent.be

Abstract

In this work, the feasibility of ultra-high drug loaded amorphous solid dispersions (ASDs) for the poorly soluble itraconazole, mebendazole and celecoxib via solvent electrospinning in combination with poly(2-ethyl-2-oxazoline) and fenofibrate in combination with polyvinylpyrrolidone is demonstrated. By lowering the polymer concentration in the electrospinning solution below its individual spinnable limit, ASDs with a drug content of up to 80 wt% are obtained. This is attributed to drug-polymer interactions not being limited by default to hydrogen bonds, as also Van der Waals interactions can result in high drug loadings. The theoretically predicted miscibility by the Flory-Huggins theory is corroborated by the experimental findings based on (modulated) differential scanning calorimetry and x-ray diffraction. Globally, the maximally obtained amorphous drug loadings are higher compared to the loadings found in literature. Additionally, non-sink dissolution tests demonstrate an increase in solubility of up to 50 times compared to their crystalline counterparts. Moreover, due to the lack of precipitation biocompatible PEtOx succeeds in stabilizing the dissolved drug and inhibiting its instant precipitation. The current work thus demonstrates the broader applicability of the electrospinning technique for the production of physically stable ASDs with ultra-high drug loadings, a result which has been validated for several Biopharmaceutics Classification System class II drugs.

Keywords

Amorphous solid dispersions (ASDs) – Poly(2-ethyl-2-oxazoline) (PEtOx) – Solvent electrospinning – Solubility enhancement – poorly soluble drugs – Flory-Huggins

Declarations of interest: JB, CV, RH and KDC are listed as inventors on a filed patent application covering high drug-loading ASD nanofibers as presented in this work. R.H. is one of the founders of Avroxa BVBA that commercializes poly(2-oxazoline)s as Ultroxa®. The other authors have no conflicts to declare.

*Corresponding authors: Karen De Clerck, Richard Hoogenboom and Chris Vervaet

Introduction

For an orally administered drug to be effective, it is crucial that the highly crystalline active pharmaceutical ingredient (API) is solubilized and absorbed by the body. Unfortunately, around 90% of the APIs in the R&D pipeline still fail to be fully commercialized, due to their lack of aqueous solubility. [1–6] Consequently, significant research has been performed and is dedicated to enhance the poor solubility of promising APIs.

One of the most studied techniques is the formation of amorphous solid dispersions (ASD). Through the amorphization of the API, the solubility and dissolution rate can be significantly improved, however, a high drug loading is often not obtained. [3,7–9] Yet, these high drug loadings are very desirable as it lowers the pill burden and increases the patient compliance. [7,10–14] Moreover, a high drug loading is also preferred from an economical point of view, as less material is needed during the formulation. [9]

Recently, the potential of the solvent electrospinning technique was demonstrated for the API flubendazole embedded in poly(2-ethyl-2-oxazoline) (PEtOx) nanofibers. [15] By solvent electrospinning a solution, which contains both the API and a polymeric excipient, a nanofibrous membrane is obtained. Typically, this membrane consists of nanofibers with a diameter below 1 µm. [16–20] Thanks to their high porosity and large specific surface area, nanofibrous nonwovens are promising for enhancing the dissolution rate of ASDs. [19–23] Moreover, the exceptionally fast solvent evaporation during solvent electrospinning kinetically entraps the API molecules within the rapidly dried polymer matrix, thus reducing the API-mobility and hindering possible re-crystallization. [15,22] It was shown that an ASD with a loading of 55 wt% was obtainable without showing signs of crystallinity according to x-ray diffraction (XRD) measurements. Moreover, significantly enhanced solubilities and increased dissolution rates compared to the crystalline API were obtained.

Interestingly, ultra-high flubendazole loadings can be achieved by lowering the PEtOx concentration below its individual electrospinnability window, due to enhanced polymer-API interactions. [15] In this contribution, the broader applicability of solvent electrospinning to manufacture PEtOx-ASDs with an ultra-high drug loading is investigated. Four model APIs, with a variety in chemical structure, were selected, namely itraconazole (ITC), mebendazole (MBZ), celecoxib (CCX) and fenofibrate (FFB), of which the chemical structures are shown in Figure 1. These APIs are classified as class II APIs according to the Biopharmaceutics Classification System (BCS), hence, they all suffer from a poor aqueous solubility. [5,24–38] It is demonstrated that the ultra-high drug loading of flubendazole in PEtOx is not a standalone case, and hydrogen bonding between polymer and API is only part of the mechanistic explanation for enhanced amorphous character.

An initial polymer-API screening is performed, both experimentally and theoretically, after which the highest possible electrospinnable drug loading is investigated and analyzed. Furthermore, the properties of the obtained electrospun ASDs are evaluated to see if the obtained nanofibrous membranes are indeed amorphous and show an increased solubility and dissolution rate compared to their crystalline pure API counterparts.

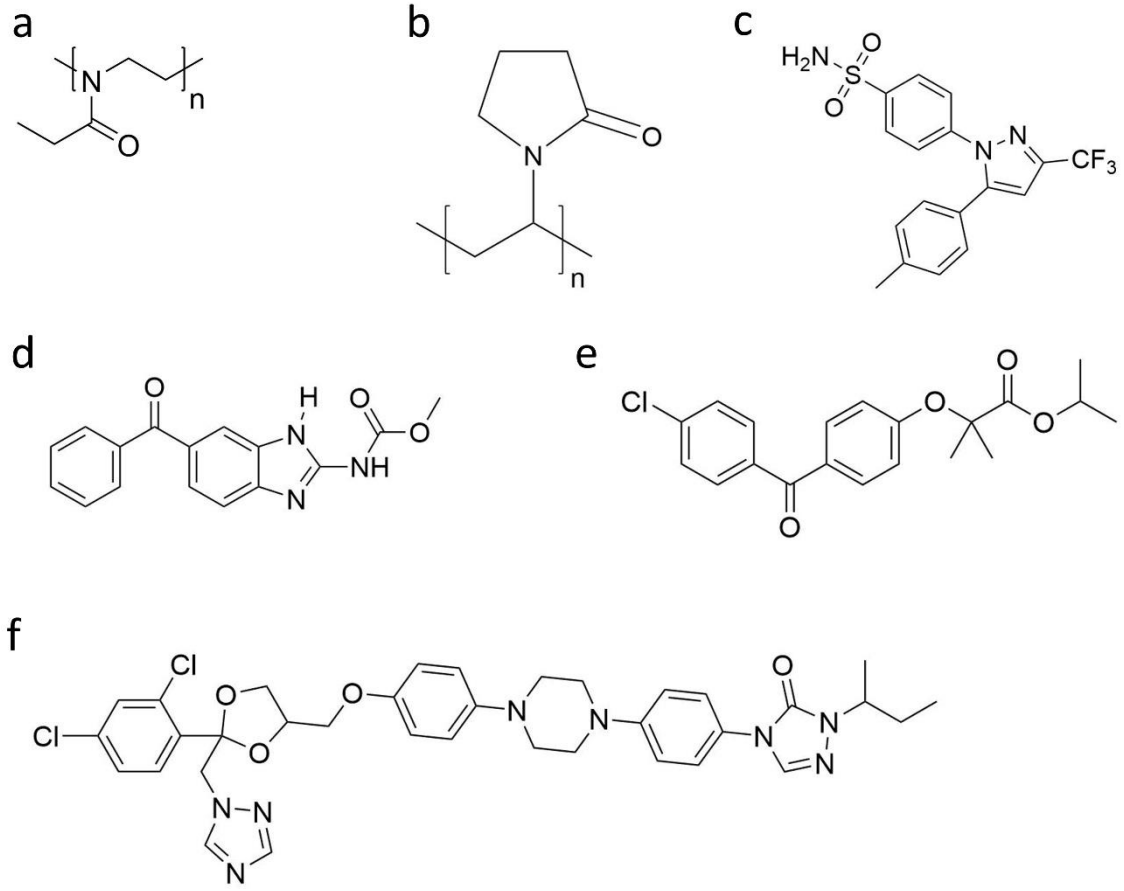

Figure 1. Chemical structures of poly(2-ethyl-2-oxazoline) (PEtOx) (a), Polyvinylpyrrolidone (PVP) (b), Celecoxib (CCX) (c), Mebendazole (MBZ) (d), Fenofibrate (FFB) (e) and Itraconazole (ITC) (f).

Materials and methods

Materials

ITC, MBZ, CCX and FFB were purchased from UTAG B.V. (Almere, Netherlands). PEtOx with a number average molar mass M_n of 62 kDa and a dispersity Đ of 1.3 was synthesized as described in literature. [15,39] Polyvinylpyrrolidone (PVP) K90 was kindly donated by BASF (Ludwigshafen, Germany). Formic acid (FA) (>98%), acetic acid (>98%) and hydrochloric acid (HCl) (37 wt% in H2O) were purchased from Sigma Aldrich (Overijse, Belgium) and used as such. Acetone was purchased from VWR International (Leuven, Belgium). All tests requiring an aqueous solution (pure H_2O or 0.1 mol L^{-1} HCl solution) were carried out with distilled water of type III as considered in ISO Standard 3696.

Electrospinning of solid dispersions

For obtaining an ultra-high drug loading the choice of solvent system is crucial since the API should be fully solubilized. As oral drug formulations are aimed for, typical hazardous solvents are avoided and only Class 3 solvents are used, which are solvents with a low toxic potential according to the ICH guideline Q3C by the European medicines agency. [40] Consequently, electrospinning solutions were prepared by dissolving different amounts of the APIs in the solvent systems shown in Table 1. After the API was fully dissolved, the polymer was added to the solution and stirred until a homogeneous, transparent solution was obtained.

Table 1. Polymer and solvent system used for the preparation of ASDs of the specified APIs (volume-based ratios)

API	Polymer	Solvent system used
Itraconazole (ITC)	PEtOx	Acetic Acid
Mebendazole (MBZ)	PEtOx	Formic Acid
Celecoxib (CCX)	PEtOx	Acetone : Acetic Acid (8:2)
Fenofibrate (FFB)	PEtOx	Acetone : Acetic Acid (8:2)
	PVP K90	Acetone : Acetic Acid (8:2)

Mass concentrations of the polymer in the electrospinning solution are expressed in weight percentages (wt%) as defined by Eq. (1) and the API content in the system (post electrospinning; again wt%) is defined by Eq. (2):

$$wt\%_{polymer} = \frac{m_{polymer}}{m_{polymer} + m_{solvent}} \quad (1)$$

$$wt\%_{API} = \frac{m_{API}}{m_{API} + m_{polymer}} \quad (2)$$

Note that the membranes can be assumed to contain the theoretical calculated API amounts and no loss of API occurred during electrospinning based on our previous work on flubendazole. [15]

All solvent electrospinning experiments were carried out using a mononozzle set-up with an 18 gauge Terumo mixing needle without bevel with a tip-to-collector distance of 15 cm. Typical electrospinning

conditions can be found in Table *2*. All electrospinning experiments were performed under climatized conditions of 25°C and 30% relative humidity in a Weisstechnik WEKK 10.50.1500 climate chamber. All electrospun samples were stored in a climatized lab at 23°C ± 1°C and a relative humidity of 25% ± 2%. All further release tests were performed on systems of maximum 2 weeks old. All membranes were electrospun at least 5 times in order to ensure reproducibility.

Table 2. Typical electrospinning conditions for the different polymer-drug systems

API	**Polymer**	**Flow rate (ml h^{-1})**	**Voltage (kV)**
ITC	PEtOx	1 ± 0.2	15 ± 3
MBZ	PEtOx	0.1 ± 0.05	20 ± 5
CCX	PEtOx	2 ± 0.5	15 ± 5
FFB	PVP K90	1 ± 0.2	10 ± 2

Scanning electron microscopy

All nanofibrous membranes were analyzed on a Phenom XL Scanning Electron Microscope (SEM) utilizing an accelerating voltage of 10 kV. Prior to analysis, the samples were coated with gold using a sputter coater (LOT MSC1T). The FiberMetric software was used to measure nanofiber diameters. All average diameters and their standard deviations were based on 500 measurements per sample.

Temperature modulated differential scanning calorimetry

Glass transition temperatures (T_g) and melting temperatures (T_m) were measured with a Temperature Modulated Differential Scanning Calorimetry (MDSC), a TA Instruments Q2000 equipped with a refrigerated cooling system (RCS90) using nitrogen as purge gas (50 mL·min^{-1}). The instrument was calibrated using Tzero technology for standard Tzero aluminum pans, using indium at the heating rate applied during the measurements. The heating rate was set at 2°C·min^{-1} and samples of 2 ± 0.5 mg were used. A heat-cool-heat procedure was used to analyze the samples, the T_g and T_m were determined with TA TRIOS software. A heat-iso temperature modulation of ± 0.32°C was selected every 60 s for FFB and the temperature was set between -60 and 120°C. For ITC, a heat-iso temperature modulation of ± 0.21°C every 40 s was selected and the temperature was set between 0 and 200°C. For MBZ, a heat-iso temperature modulation of ± 0.32°C every 60 s was selected and the temperature was set between -20 and 120°C. For CCX, a heat-iso temperature modulation of ± 0.32°C every 60 s was selected and the temperature was set between -20 and 220°C. Experiments were performed in triplicate.

X-ray diffraction

All ASDs were measured as such employing an ARL™ X'TRA Powder Diffractometer of Thermo Scientific. The monochromatic X-rays are produced by a copper X-ray tube, with Cu K-shell energy levels are equivalent to λ = 0.154056 nm. The diffraction patterns were recorded at an interval of 5 to 60 ° 2θ with a step size of 0.02 ° and a measuring time of 45 min. A Si (Li) solid-state detector was used for data collection. To determine the sensitivity of the diffractometer towards the crystalline API, physical mixtures (PM) of PEtOx and API were prepared and measured accordingly.

In vitro dissolution tests under non-sink conditions

For both the pure APIs and the produced ASDs *in vitro* dissolution tests were performed in 0.1 mol L^{-1} HCl. An equivalent of 50 mg of API was added in baskets to a 200 ml 0.1 mol L^{-1} HCl, pH 1, dissolution medium. The medium was stirred at a constant speed of 100 rpm and samples of 1 ml were taken at different time intervals, *i.e.* 3, 5, 10, 15, 30, 60, 90, 120, 180 and 300 minutes. Samples were filtered through a 0.45 µm PTFE filter, diluted to fit the calibration solution (as discussed in the UV-visible spectroscopy section) and measured via UV-visible spectroscopy. Experiments were performed in triplicate.

UV-visible spectroscopy

A double beam Perkin-Elmer Lambda 900 UV-Vis spectrophotometer in transmission mode was used to record UV-Vis spectra. The spectra were recorded from 250 nm to 400 nm with a data interval of 1 nm. Calibration curves were made and used to relate the absorbance of the APIs to their concentration in solution. To prepare these calibration curves, a solution was searched for that was able to dissolve a sufficient amount of crystalline API. For itraconazole this was a solution of 100 ml 0.1 mol L^{-1} HCl and 2 ml of acetic acid, for celecoxib 100 ml 0.1 mol L^{-1} HCl and 20 ml of acetic acid was used and for mebendazole a solution of 100 ml 0.1 mol L^{-1} HCl and 2 ml of formic acid was used to prepare the calibration curve. Through a fitting dilution media, all samples were measured in the same solution as used for the calibration curves.

Results and discussion

Polymer-API screening based on glass transition temperature calculations

The preservation of the optimal storage conditions is one of the requirements in order to obtain a time-stable, and thus durable ASD. Specifically, a steady low relative humidity is essential, as moisture can induce mobility of the molecules, resulting in crystallization. [6,41–44] It is hence essential to understand polymer and API interplay, such as drug-polymer miscibility and interactions. [6,41,45,46] These can be screened by for instance, the T_g being single or dual mode, which is an indication of molecular mobility and, hence, of the kinetic stability of the ASD. Above T_g there is an increased

molecular mobility, enabling (natural longer term) reorganization of the API molecules and their subsequent crystallization, while below T_g the system has a reduced mobility and is kinetically stabilized. [32,47,48] In many cases, this T_g on the level of the ASD is theoretically calculated via the Fox equation (Eq. 3) and the Gordon-Taylor equation (Eq. 4). [11,49–51]

$$\frac{1}{T_g} = \frac{w_1}{T_{g1}} + \frac{w_2}{T_{g2}} \tag{3}$$

$$T_g = \frac{w_1 T_{g1} + k w_2 T_{g2}}{w_1 + k w_2} \tag{4}$$

in which w_i and T_{gi} are the respective weight fraction and glass transition of the pure components. In Eq. 4, the *k* value is a measure for the difference in expansion in the rubbery and glassy state of the pure components. [52] Note that extra interaction terms are not included and thus deviations between experiment and theory should be interpreted in this manner, *i.e*. the establishment of *e.g.* interactions between API and polymer.

An initial screening based on Eq. 3 and 4 for the four APIs under consideration, *i.e*. FFB, ITC, CCX and MBZ, and two polymeric excipients, *i.e.* poly(2-ethyl-2-oxazoline) (PEtOx) and polyvinylpyrrolidone grade K90® (PVP K90), results in the values given in Table 3. Only for the PEtOx-FFB systems a T_g below room temperature is obtained, indicating that only an ASD of PEtOx-FFB is kinetically not feasible and one should be careful with the use of FFB. Therefore, PVP was looked at as an alternative excipient. A solid dispersion of FFB together with PVP K90 is indeed already characterized by a T_g above 50°C according to both the Fox and Gordon-Taylor equation considering 50 wt% fenofibrate in the ASD. Hence, stable FFB ASDs should be feasible with PVP K90 as excipient. This is a result of the higher T_g of PVP K90 compared to that of PEtOx, 180°C *vs.* 62°C. For the three other APIs, *i.e.* ITC, MBZ and CCX, kinetic stabilization seems possible in combination with PEtOx (theoretical T_g > room temperature).

Table 3. Theoretical Tg screening of possible polymer-API combinations at an API concentration of 50 wt% (Eq. (3) and (4)).

API	T_g API (°C)	Polymer	T_g polymer (°C)	T_g according to Fox (°C)	T_g according to Gordon-Taylor (°C)	k
ITC	60	PEtOx	62	61	60	1.1
MBZ	114	PEtOx	62	86	83	0.7
CCX	59	PEtOx	62	60	61	1.4
FFB	-18.5	PEtOx	62	16	7	2.1
FFB	-18.5	PVP K90	180	53	52	1.8

Polymer-API screening based on Flory-Huggins theory

Aside from kinetic stability, for long-term stability, thermodynamics play an important role. One needs to know if polymer-API blends are miscible, or if phase separation is eventually inevitable. To examine the polymer-API miscibility, the Flory-Huggins (FH) theory is widely used. This theory is an extension of the lattice theory for regular solutions, accounting for the connectivity of monomer units from a statistical thermodynamic point of view. [6,7,16,47,53–58] One of the downsides of the FH theory is that interactions such as hydrogen bonding and ionic interactions are by default not considered. However, for two of the four APIs under consideration these interactions are not expected, namely for FFB and ITC. [57,59]

The polymer-API miscibility is dependent on the molar Gibbs free energy change upon mixing, ΔG^*_m, which, according to the FH theory, can be calculated according to Eq. 5:

$$\Delta G_m^* = RT \left[\phi_1 \, ln(\phi_1) + \frac{\phi_2}{x_n} ln(\phi_2) + \phi_1 \phi_2 \chi\right] \quad (5)$$

with *R* and *T* the universal gas constant and the absolute temperature, ϕ_1 and ϕ_2 the volume fractions of API and polymer respectively, and x_n the number average (segment/chain) length of the polymer, with each segment formally equal in size to an API molecule. Furthermore, χ represents the Flory-Huggins interaction parameter, a temperature-dependent dimensionless quantity that characterizes polymer-API interactions. [53,59–62] For a blended system to be thermodynamically miscible, a negative ΔG^*_m is required.

From Eq. 5 it is clear that χ is crucial in obtaining a negative ΔG^*_m. Several experimental options exist to determine χ, however, due to the amorphous nature of PEtOx, χ is herein theoretically determined through the solubility parameter approach according to Eq. 6.

$$\chi = \frac{V_{site}(\delta_1 - \delta_2)^2}{RT} + \beta \quad (6)$$

with V_{site} the (average) molar volume and β the entropic lattice constant and δ_i the solubility parameter of the polymer and the API. [43,59,62] It has been reported, however, that for non-polar mixtures a better correlation is found in case β equals zero, reducing Eq. 4 to the Hildebrand's equation for regular solutions. [63] For the systems under consideration, with the parameters provided in Section S1 of the Supporting Information differentiating at least for the delta values between dispersion forces, polar forces and the contribution of hydrogen bonding, FFB and PVP K90 pair immiscibility is first indicated by the large difference in Hansen Δδ (>7) (see Table S1.1). Additionally, the FH theory shows an unfavorable mixing of FFB and PVP K90, with phase separation predicted to occur from 5 wt% of FFB in the ASD onwards, see Figure 2 (a). Hence, the direct use of FFB is again proven to be questionable.

Notably, as shown in Figure 2 (b), thermodynamically stable ASDs with high drug loadings are expected to occur for PEtOx ASD systems with ITC (up to 60 wt%), CCX (up to 84 wt%) and MBZ (no phase separation predicted according to FH theory).

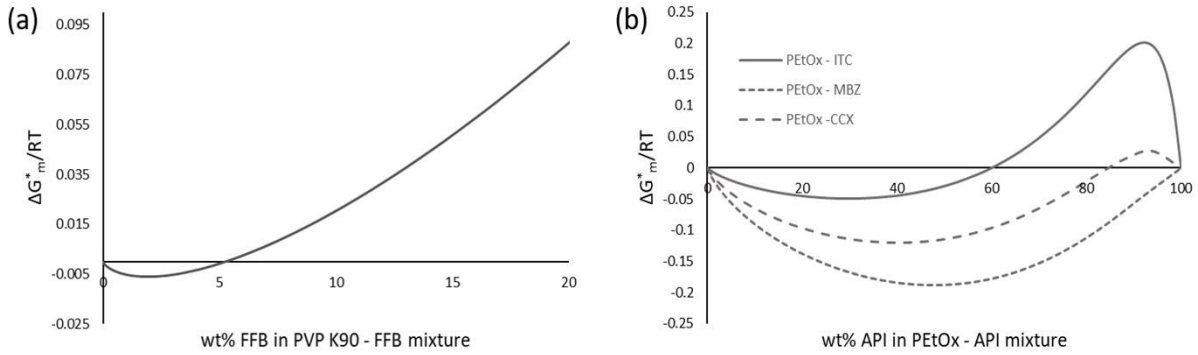

Figure 2. Thermodynamic miscibility according to FH theory by means of a (reduced) ΔG^*_m vs. API wt% plot for the different polymer-API systems. (a) shows the PVP K90 – FFB system. Phase separation is expected to occur at 5 wt% of FFB. (b) shows the thermodynamic miscibility of PEtOx-ITC (full line), PEtOx-MBZ (dotted line) and PEtOx-CCX (striped line). All three systems are expected to remain miscible until a high drug loading of 60 wt% for ITC, 84 wt% for CCX and for MBZ no phase separation is expected at all.

Maximal electrospinnable drug loading

As previously mentioned, a high drug loading is desired from both an economical point of view as well as for patient compliance. Therefore, the highest possible electrospinnable loading for each polymer-API system was investigated. Table 3 highlights for the PEtOx-FFB system a high degree of molecular mobility, so that it can be understood why the electrospun membrane quickly loses its morphology and turns into a film. This is shown in Figure S2.1, and explains why this system will not be further investigated.

Fortunately, the other systems in Table 3 are different in molecular stability. Moreover, based on the insights gained in previous research, a polymer concentration was used, for both PEtOx and PVP K90, which is below the individual electrospinnable window. [15] Doing so, solvent electrospun ASDs with ultra-high drug loadings of at least 60 wt% and even up to 85 wt% were obtained, as shown in Figure 3. A more detailed analysis of the electrospinnable window of the ASD systems can be found in Figure S2.2, Figure S2.3, Figure S2.4 and Figure S2.5 of the Supporting Information. It is hypothesized that for these systems additional inter-chain interactions and entanglements are created, thereby sufficiently increasing the viscosity to still allow a stable electrospinning process despite less polymer being present. Previous work hypothesized that this is due to hydrogen bonding occurring between polymer and API, however, for both FFB and ITC significant hydrogen bonding is unlikely with PEtOx nor PVP. Consequently, it can be concluded that the interactions that allow for added inter-chain interactions and entanglements do not strictly need to be hydrogen bonds between the polymer and the API. They

could also result from other interactions such as hydrogen bonding with the solvent or Van der Waals interactions.

API-polymer system	ITC-PEtOx	MBZ-PEtOx	CCX-PEtOx	FFB-PVP K90
Maximal loading (wt%)	80	70	85	60
SEM image of maximal loading	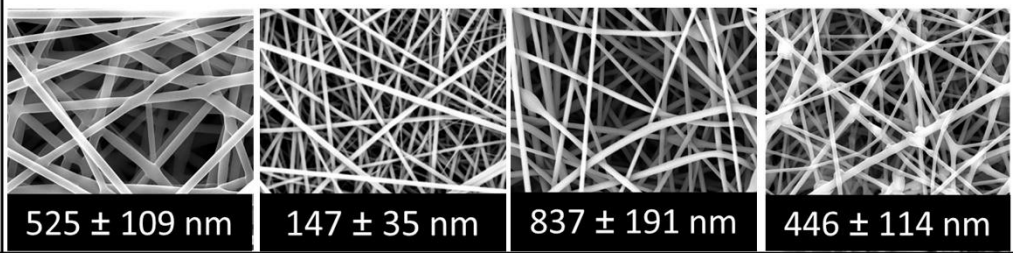			
	525 ± 109 nm	147 ± 35 nm	837 ± 191 nm	446 ± 114 nm

Figure 3. An overview of the highest drug loadings that still resulted in electrospinnable solutions. Increasing the drug loading even more resulted in solutions that were not electrospinnable.

Evaluation of the amorphous nature and kinetic stability via MDSC and XRD analysis

To validate the miscibility results obtained by the FH theory (interpretation of Figure 2), the amorphous nature of the obtained ASDs was analyzed through modulated differential scanning calorimetry (MDSC) and x-ray diffraction (XRD) analysis. In a first step, Figure 4 demonstrates the validity of the FH theory for PVP K90 – FFB (5% threshold). A distinct Bragg peak, as benchmarked by the 5 wt% physical (test) mixture PM (no fibers), is seen for both the 40 and 50 wt% nanofibrous membrane, indicating crystallinity after one month of storage (23 ± 1°C and a relative humidity of 25 ± 2%). Moreover, the MDSC data clearly show the presence of a double FFB melting peak, without the occurrence of cold crystallization prior to the melt. Further analysis of the DSC data, using the melting enthalpy of the ASD compared to that of the melting of the pure component, reveals that there is already 4.2 wt% of crystalline FFB present in the nanofibrous membrane, which is around 10% of the total FFB fraction, as shown in Table 4. As such, the high immiscibility between FFB and PVP K90 is not solely theoretically predicted, but experimentally observed as well.

Table 4. Overview of the melting enthalpies for PVP K90 – FFB ASDs obtained by the MDSC analysis. The fraction of crystallized FFB was calculated and given as well. It is clear that at 40 wt% there is already a significant amount of crystalized FFB present in the nanofibrous membrane.

wt% FFB	Melting enthalpy (J g^{-1})	wt% crystalline FFB
40	9.5	4.2
50	14.4	8.1
60	21.4	14.4
100	89.1	100

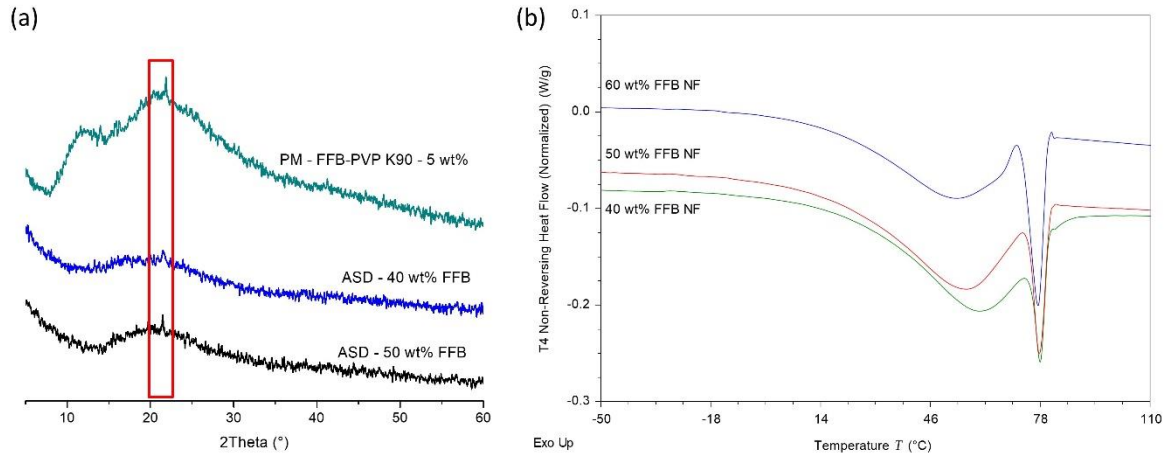

Figure 4. a: X-ray diffractogram of PVP K90 – FFB 40 and 50 wt% ASDs and a 5 wt% PM (physical mixture: no fibers). It is clear that the 40 wt% ASD already results in a certain degree of crystallinity as seen by the presence of a Bragg peak at 21° (2θ). This result is corroborated by the presence of a distinct melting peak in the non-reversing MDSC thermogram. (b) All measurements were performed on systems of maximum 2 weeks old.

In a second step, it follows that the XRD and MDSC data obtained for the other systems, PEtOx-ITC, PEtOx-MBZ and PEtOx-CCX, corroborate the FH theory as well, as shown in Figure 5. No distinct Bragg peaks are seen for any of the nanofibrous ASDs, so that the amorphous nature of the ASDs is underpinned. Moreover, MDSC analysis reveals a single T_g for all nanofibrous ASDs, which means no detectable amorphous-amorphous phase separation has occurred. Furthermore, a positive deviation in the T_g value is observed compared to the theoretical values obtained by Fox equation (Eq. 3), suggesting that there are interactions present between PEtOx and the API. For PEtOx–CCX ASDs a positive deviation of nearly 20°C is even observed, indicating a strong kinetic stabilization of the ASD due to strong polymer-API interactions being present. For both MBZ and CCX the interactions at play are hypothesized to be hydrogen bonds, whereas for PEtOx–ITC only Van der Waals forces are expected, with dipole-dipole interactions probably being the most important ones. Although the 70 wt% ITC ASD appears to be fully amorphous according to XRD, MDSC analysis reveals a melting peak

(Figure S3.1 of the Supporting Information), indicating that 2% of the ITC is in its crystalline form. The same is noticed for 85 wt% CCX (Figure S3.2 of the Supporting Information). For this high drug content, 8% of the CCX is in the crystal state.

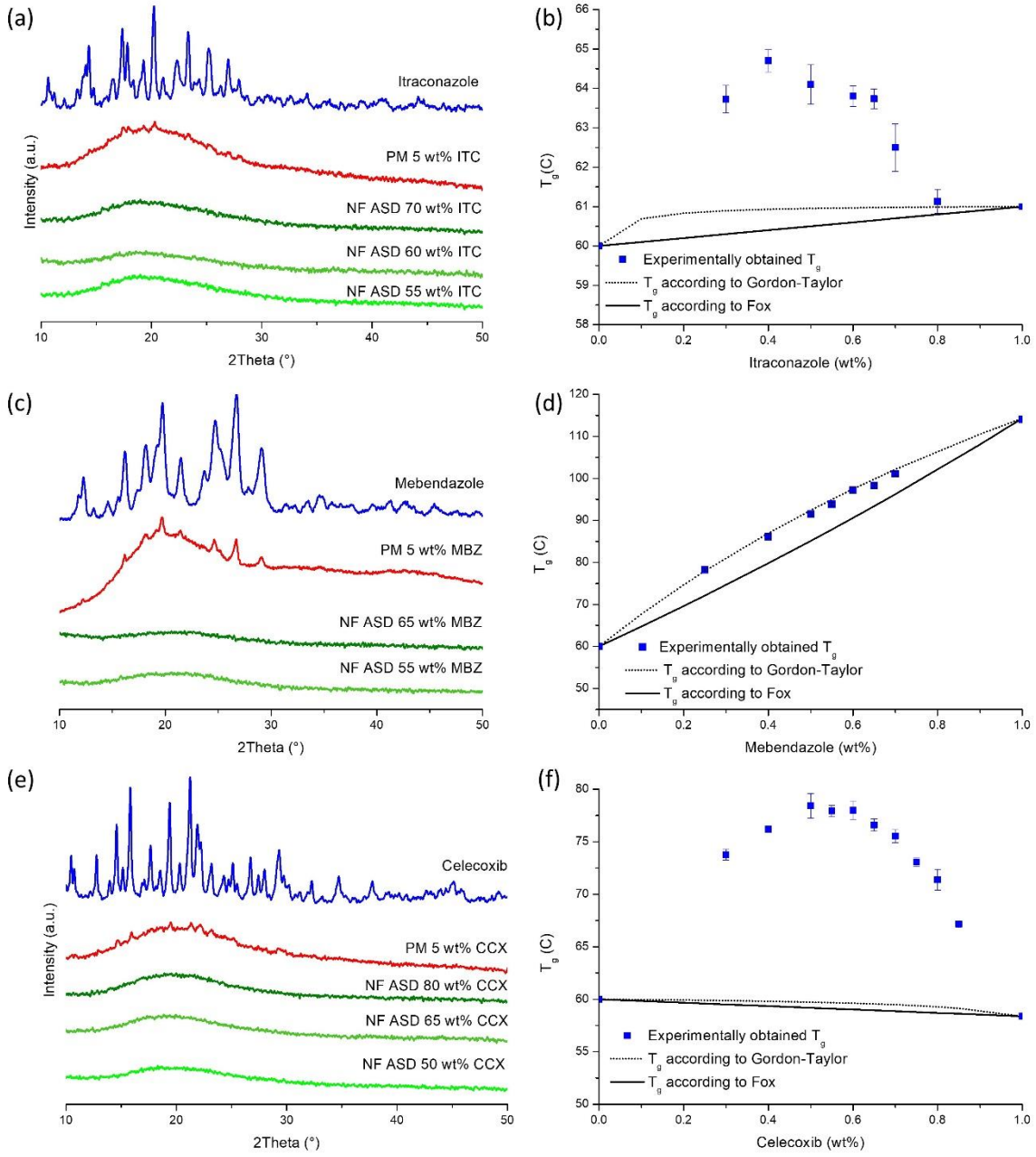

Figure 5. Overview of x-ray diffractograms (a, c, e) and T_g measurement (b, d, f) of the different PEtOx-API systems. a and b show the results for the PEtOx – ITC ASDs, c and d for the PEtOx – MBZ ASDs and e and f show the results for the PEtOx – CCX ASDs. For all x-ray diffractograms a physical mixture (PM) containing 5 wt% API is included to ensure the sensitivity of the measurement, all PMs show distinct Bragg peaks related to the pattern of the pure API, which do not show up for any of the nanofibrous (NF) ASDs, revealing their amorphous nature. All thermograms show the measured T_g values and their standard deviation (n=3), these values are compared to theoretical values according to Eq. 3 (Fox) and Eq. 4 (Gordon-Taylor) (parameters in Table 3). All T_g values show a positive deviation from the theoretical Fox equation indicating the presence of supportive interactions between PEtOx and API. All measurements were performed on systems of maximum 2 weeks old.

It ought to be noted that this crystallinity is not observed for lower wt%, indicating amorphous ASDs. In addition, heat-iso modulation conditions were used during all MDSC measurements. As such, the modulation is unable to induce crystallization, thus allowing for accurate melting and crystallization analysis. Hence, although the FH theory is known to have its drawbacks, we do see a good fit between the theoretically predicted and the experimentally observed miscibility.

Table 5 gives an overview of the results of the current work and the field. Here, the true potential of the solvent electrospinning technique is revealed, as it clearly enables the production of ASDs with ultra-high drug loadings, which are significantly higher than those found in literature. Only for FFB no fully amorphous ASD could be obtained, due to kinetic instability with PEtOx, as indicated by the low T_g, and polymer-API immiscibility with PVP K90 as excipient, as indicated by the MDSC results. To realize these unprecedented results, the reduction of the polymer concentration below its electrospinnable limit is crucial for obtaining the ultra-high drug loadings.

Table 5: Overview of the maximal obtained amorphous drug loadings through the solvent electrospinning technique, compared to the maximal drug loadings obtained in literature for these APIs through various other techniques.

Polymer-API system	**Maximal obtained drug loading (wt%)**	**Maximal obtained amorphous drug loading (wt%)**	**Determining factor**	**Maximal drug loading found in literature (wt%)**	**Maximal amorphous drug loading found in literature (wt%)**
ITC-PEtOx	80	60	Crystallinity	40 – 60[2,28,64,65]	50[2,28]
MBZ-PEtOx	70	70	Spinnable limit	50[34,66]	20[34,66]
CCX-PEtOx	85	80	Crystallinity	40 – 70[67–69]	70[69]
FFB-PEtOx	x	X	Loss of fiber morphology due to Tg	30 – 40[2,32,70–72]	40[32]
FFB-PVP K90	60	x	Crystallinity		

Non-Sink in vitro dissolution

After showing the promising potential of solvent electrospinning for obtaining fully amorphous ASDs with a high drug loading, it is crucial to investigate their dissolution behavior as well. *In vitro* non-sink dissolution tests demonstrate a significantly increased solubility and enhanced dissolution rate compared to the pure crystalline API (Figure 6). As summarized in Table 6, the ASDs resulted in a 25, 18 and 15-fold higher API release after 1 hour compared to the dissolution of the crystalline API for respectively ITC (a), CCX (b) and MBZ (C).

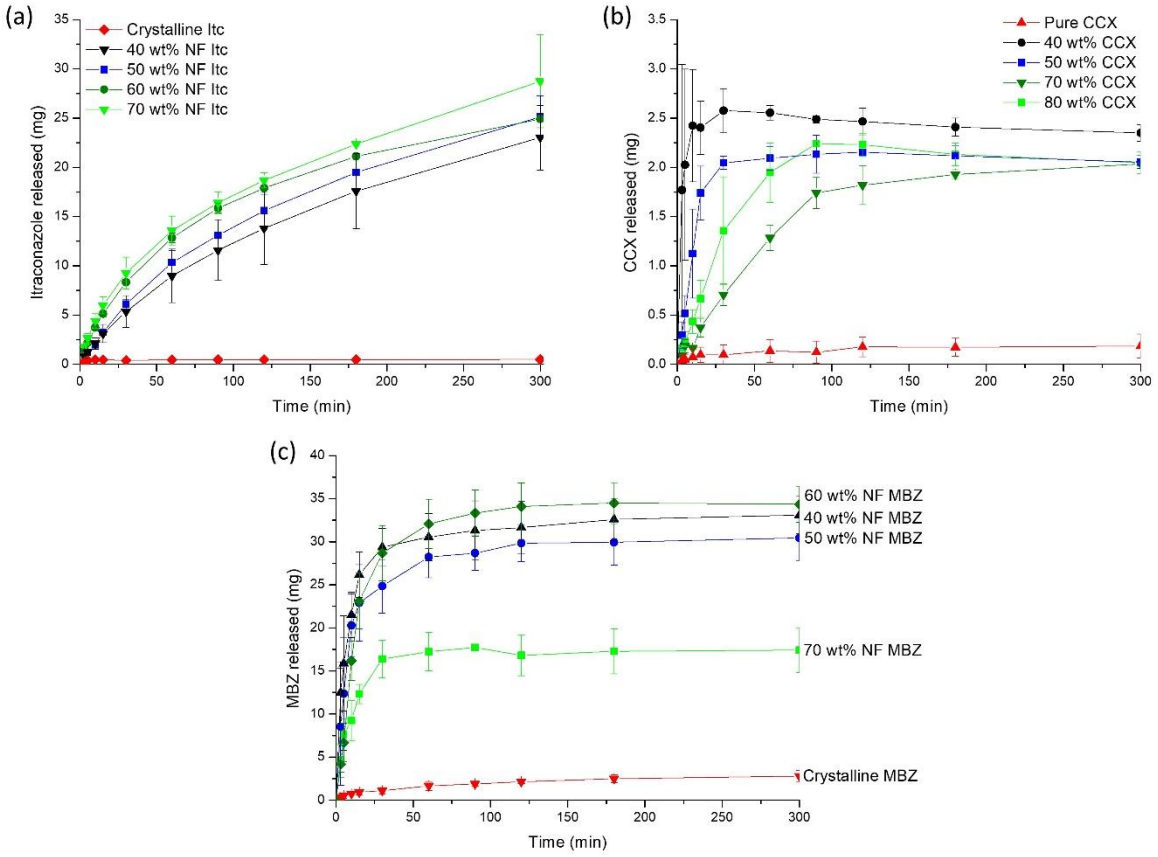

Figure 6. Dissolution results for the non-sink in vitro tests for the PEtOx – ICT (a), – CCX (b) and – MBZ (c) ASDs. A clear increase in dissolution rate and solubility of the APIs is observed, indicating the promise of the solvent electrospinning technique for enhancing the bioavailability of poorly soluble APIs. All measurements were performed in triplicate. All measurements were performed on systems of maximum 2 weeks old.

It is clear that the formation of nanofibrous ASDs facilitates the release of poorly soluble APIs, thus increasing their bioavailability. Note that for ITC, the maximal solubility has not been reached even after five hours, not even for the 70 wt% loading. Although DSC measurements revealed this ASD to be on the verge of being fully amorphous, with only a 2% crystallinity, it still behaves identical to the lower wt% PEtOx-ITC ASDs. For PEtOx-CCX ASDs, a plateau dissolution is reached within the first two hours, independent of the drug loading. It should be noted that the rate to reach this plateau is remarkably faster for the 40 and 50 wt% ASDs, which could be related to their smaller (average)

nanofiber diameter, 741 and 1030 nm vs. 1481 and 1630 nm (70 and 80 wt%). For the PEtOx-MBZ ASDs, it is notable that the 70 wt% MBZ ASD exhibits a remarkably lower MBZ release compared to MBZ ASDs with a lower API content. It is assumed that this is due to re-crystallization of the API prior or during API dissolution. This was also seen visually after the test, with significantly more of the sample not disintegrating for the 70 wt% membrane compared to the lower drug contents.

Nonetheless, for all ASDs, no significant drop in released API is noticed (Figure 6), even after five hours, indicating that no API precipitation occurred. These results demonstrate the ability of PEtOx to prevent precipitation of the APIs under supersaturated conditions.

Table 6. Summary of amounts of API released after 1 hour and 5 hours. A significant increase in API release is measured when formulated as a nanofibrous ASD.

	Itraconazole release (mg)	**Mebendazole release (mg)**	**Celecoxib release (mg)**
Crystalline 1h	0.5	1.7	0.1
Average ASD 1h	11.5	29.7	2.0
Factor increased	***25***	***18***	***15.***
Crystalline 5h	0.5	2.8	0.2
Average ASD 5h	25.7	31.9	2.1
Factor increased	***51***	***11***	***12***

Conclusions

The formulation of ASDs with a high drug loading is challenging. In this study it is shown that obtaining ultra-high drug loaded electrospun ASD nanofibers is possible for a wide range of polymer-API systems. In order to obtain high drug contents above 40 wt%, it is crucial to lower the polymer concentration in the electrospinning solution below its individual spinnable limit.

It is hypothesized that the use of lower polymer amounts is feasible due to the strong interactions between polymer and API. It was shown for ITC and FFB that these interactions do not need to be hydrogen bonds, but also Van der Waals dipolar forces can provide sufficient interaction to result in additional inter-chain interactions and entanglements. Despite that the FH theory faces limitations, especially combined with the use of solubility parameters, a good fit was obtained with the experimental data. This indicates the relevance of the theory as a screening tool.

Overall, it can be concluded that the biocompatible PEtOx succeeded in stabilizing the dissolved API and inhibiting its instant precipitation under supersaturated conditions, as is the case for non-sink dissolution. The electrospinning technique provides vital features for obtaining physically stable ASDs

with ultra-high drug loadings. These results are obtained for multiple APIs, thus indicating the potential broader applicability to other BCS class II and IV APIs.

Acknowledgements

Financial support from the Research Foundation – Flanders (FWO) is gratefully acknowledged for funding the research through SB PhD grants 1S89118N of JB and 1S22722N of OF. Ghent University is also thanked by KDC, RH, D.R.D. and CV for its continued support. Additionally, Tijs Redant is thanked for performing experiments.

References

[1] S. V. Bhujbal, B. Mitra, U. Jain, Y. Gong, A. Agrawal, S. Karki, L.S. Taylor, S. Kumar, Q. (Tony) Zhou, Pharmaceutical amorphous solid dispersion: A review of manufacturing strategies, Acta Pharm. Sin. B. 11 (2021) 2505–2536. https://doi.org/10.1016/j.apsb.2021.05.014.

[2] E. Boel, A. Smeets, M. Vergaelen, V.R. De la Rosa, R. Hoogenboom, G. Van den Mooter, Comparative study of the potential of poly(2-ethyl-2-oxazoline) as carrier in the formulation of amorphous solid dispersions of poorly soluble drugs, Eur. J. Pharm. Biopharm. 144 (2019) 79–90. https://doi.org/10.1016/j.ejpb.2019.09.005.

[3] D.H. Kim, Y.W. Kim, Y.Y. Tin, M.T.P. Soe, B.H. Ko, S.J. Park, J.W. Lee, Recent technologies for amorphization of poorly water-soluble drugs, Pharmaceutics. 13 (2021). https://doi.org/10.3390/pharmaceutics13081318.

[4] S. Kalepu, V. Nekkanti, Insoluble drug delivery strategies: Review of recent advances and business prospects, Acta Pharm. Sin. B. 5 (2015) 442–453. https://doi.org/10.1016/j.apsb.2015.07.003.

[5] T. Xie, L.S. Taylor, Improved release of celecoxib from high drug loading amorphous solid dispersions formulated with polyacrylic acid and cellulose derivatives, Mol. Pharm. 13 (2016) 873–884. https://doi.org/10.1021/acs.molpharmaceut.5b00798.

[6] M. Davis, G. Walker, Recent strategies in spray drying for the enhanced bioavailability of poorly water-soluble drugs, J. Control. Release. 269 (2018) 110–127. https://doi.org/10.1016/j.jconrel.2017.11.005.

[7] H. Grohganz, P.A. Priemel, K. Löbmann, L.H. Nielsen, R. Laitinen, A. Mullertz, G. Van den Mooter, T. Rades, Refining stability and dissolution rate of amorphous drug formulations, Expert Opin. Drug Deliv. 11 (2014) 977–989. https://doi.org/10.1517/17425247.2014.911728.

[8] T. Vigh, B. Démuth, A. Balogh, D.L. Galata, I. Van Assche, C. Mackie, M. Vialpando, B. Van Hove, P. Psathas, E. Borbás, H. Pataki, P. Boeykens, G. Marosi, G. Verreck, Z.K. Nagy, Oral bioavailability enhancement of flubendazole by developing nanofibrous solid dosage forms, Drug Dev. Ind. Pharm. 9045 (2017) 1–8. https://doi.org/10.1080/03639045.2017.1298121.

[9] A. Schulz, S. Jaksch, R. Schubel, E. Wegener, Z. Di, Y. Han, A. Meister, J. Kressler, A. V. Kabanov, R. Luxenhofer, C.M. Papadakis, R. Jordan, Drug-induced morphology switch in drug delivery systems based on poly(2-oxazoline)s, ACS Nano. 8 (2014) 2686–2696. https://doi.org/10.1021/nn406388t.

[10] S. V. Jermain, C. Brough, R.O. Williams, Amorphous Solid Dispersions and Nanocrystal Technologies for Poorly Water-Soluble Drug Delivery – An Update, Int. J. Pharm. 535 (2017) 379–392. https://doi.org/10.1016/j.ijpharm.2017.10.051.

[11] S. Janssens, G. Van den Mooter, Review: physical chemistry of solid dispersions, J. Pharm. Pharmacol. 61 (2009) 1571–1586. https://doi.org/10.1211/jpp/61.12.0001.

[12] H.J. Kwon, E.J. Heo, Y.H. Kim, S. Kim, Y.H. Hwang, J.M. Byun, S.H. Cheon, S.Y. Park, D.Y. Kim, K.H. Cho, H.J. Maeng, D.J. Jang, Development and evaluation of poorly water-soluble celecoxib as solid dispersions containing nonionic surfactants using fluidized-bed granulation, Pharmaceutics. 11 (2019). https://doi.org/10.3390/pharmaceutics11030136.

[13] M.M. Knopp, J. Wendelboe, R. Holm, T. Rades, Effect of amorphous phase separation and crystallization on the in vitro and in vivo performance of an amorphous solid dispersion, Eur. J. Pharm. Biopharm. 130 (2018) 290–295. https://doi.org/10.1016/j.ejpb.2018.07.005.

[14] S. Dedroog, C. Huygens, G. Van den Mooter, Chemically identical but physically different: A comparison of spray drying, hot melt extrusion and cryo-milling for the formulation of high drug loaded amorphous solid dispersions of naproxen, Eur. J. Pharm. Biopharm. 135 (2019). https://doi.org/10.1016/j.ejpb.2018.12.002.

[15] J. Becelaere, E. Van Den Broeck, E. Schoolaert, J.F.R. Van Guyse, M. Vergaelen, S. Borgmans, K. Creemers, V. Van Speybroeck, C. Vervaet, R. Hoogenboom, K. De Clerck, Stable amorphous solid dispersion of flubendazole with high loading via electrospinning, 351 (2022) 123–136. https://doi.org/10.1016/j.jconrel.2022.09.028.

[16] K. Göke, T. Lorenz, A. Repanas, F. Schneider, D. Steiner, K. Baumann, H. Bunjes, A. Dietzel, J.H. Finke, B. Glasmacher, A. Kwade, Novel strategies for the formulation and processing of poorly water-soluble drugs, Eur. J. Pharm. Biopharm. 126 (2018) 40–56. https://doi.org/10.1016/j.ejpb.2017.05.008.

[17] L. Shang, Y. Yu, Y. Liu, Z. Chen, T. Kong, Y. Zhao, Spinning and applications of bioinspired fiber systems, ACS Nano. 13 (2019) 2749–2772. https://doi.org/10.1021/acsnano.8b09651.

[18] S. Sabra, D.M. Ragab, M.M. Agwa, S. Rohani, Recent advances in electrospun nanofibers for some biomedical applications, Eur. J. Pharm. Sci. 144 (2020) 105224. https://doi.org/10.1016/j.ejps.2020.105224.

[19] K.S. Ogueri, C.T. Laurencin, Nanofiber technology for regenerative engineering, ACS Nano. 14 (2020) 9347–9363. https://doi.org/10.1021/acsnano.0c03981.

[20] A. Luraghi, F. Peri, L. Moroni, Electrospinning for drug delivery applications: A review, J. Control. Release. 334 (2021) 463–484. https://doi.org/10.1016/j.jconrel.2021.03.033.

[21] T.J. Sill, H.A. von Recum, Electrospinning: Applications in drug delivery and tissue engineering, Biomaterials. 29 (2008) 1989–2006. https://doi.org/10.1016/j.biomaterials.2008.01.011.

[22] D.G. Yu, J.J. Li, G.R. Williams, M. Zhao, Electrospun amorphous solid dispersions of poorly water-soluble drugs: A review, J. Control. Release. 292 (2018) 91–110. https://doi.org/10.1016/j.jconrel.2018.08.016.

[23] S. Thakkar, M. Misra, Electrospun polymeric nanofibers: New horizons in drug delivery, Eur. J. Pharm. Sci. 107 (2017). https://doi.org/10.1016/j.ejps.2017.07.001.

[24] F. Theil, J. Milsmann, S. Anantharaman, H. Van Lishaut, Manufacturing Amorphous Solid Dispersions with a Tailored Amount of Crystallized API for Biopharmaceutical Testing, Mol. Pharm. 15 (2018) 1870–1877. https://doi.org/10.1021/acs.molpharmaceut.8b00043.

[25] C. Phadke, J. Sharma, K. Sharma, A.K. Bansal, Effect of Variability of Physical Properties of Povidone K30 on Crystallization and Drug-Polymer Miscibility of Celecoxib-Povidone K30 Amorphous Solid Dispersions, Mol. Pharm. 16 (2019) 4139–4148.

https://doi.org/10.1021/acs.molpharmaceut.9b00452.

[26] P.D. Nunes, J.F. Pinto, J. Henriques, A.M. Paiva, Insights into the release mechanisms of ITZ:HPMCAS amorphous solid dispersions: The role of drug-rich colloids, Mol. Pharm. 19 (2022) 51–66. https://doi.org/10.1021/acs.molpharmaceut.1c00578.

[27] M. Van Speybroeck, R. Mols, R. Mellaerts, T. Do Thi, J.A. Martens, J. Van Humbeeck, P. Annaert, G. Van den Mooter, P. Augustijns, Combined use of ordered mesoporous silica and precipitation inhibitors for improved oral absorption of the poorly soluble weak base itraconazole, Eur. J. Pharm. Biopharm. 75 (2010) 354–365. https://doi.org/10.1016/j.ejpb.2010.04.009.

[28] V. Bhardwaj, N.S. Trasi, D.Y. Zemlyanov, L.S. Taylor, Surface area normalized dissolution to study differences in itraconazole-copovidone solid dispersions prepared by spray-drying and hot melt extrusion, Int. J. Pharm. 540 (2018) 106–119. https://doi.org/10.1016/j.ijpharm.2018.02.005.

[29] R. Takano, R. Maurer, L. Jacob, F. Stowasser, C. Stillhart, S. Page, Formulating Amorphous Solid Dispersions: Impact of Inorganic Salts on Drug Release from Tablets Containing Itraconazole-HPMC Extrudate, Mol. Pharm. 17 (2020) 2768–2778. https://doi.org/10.1021/acs.molpharmaceut.9b01109.

[30] M.T. Davis, C.B. Potter, M. Mohammadpour, A.B. Albadarin, G.M. Walker, Design of spray dried ternary solid dispersions comprising itraconazole, soluplus and HPMCP: Effect of constituent compositions, Int. J. Pharm. 519 (2017) 365–372. https://doi.org/10.1016/j.ijpharm.2017.01.043.

[31] M. Van Speybroeck, R. Mellaerts, R. Mols, T. Do Thi, J.A. Martens, J. Van Humbeeck, P. Annaert, G. Van den Mooter, P. Augustijns, Enhanced absorption of the poorly soluble drug fenofibrate by tuning its release rate from ordered mesoporous silica, Eur. J. Pharm. Sci. 41 (2010) 623–630. https://doi.org/10.1016/j.ejps.2010.09.002.

[32] C.N. Nguyen, C.V. Pham, G. Le Thien, B.T. Ngoc, H. Le Thi, C.P.T. Huyen, T.N. Thi, Immediate-released pelletized solid dispersion containing fenofibrate: Formulation, in vitro characterization, and bioequivalence studies in experimental beagle dogs, Int. J. Pharm. 570 (2019) 118661. https://doi.org/10.1016/j.ijpharm.2019.118661.

[33] N.Q. Shi, S.R. Wang, Y. Zhang, J.S. Huo, L.N. Wang, J.H. Cai, Z.Q. Li, B. Xiang, X.R. Qi, Hot melt extrusion technology for improved dissolution, solubility and “spring-parachute” processes of amorphous self-micellizing solid dispersions containing BCS II drugs indomethacin and fenofibrate: Profiles and mechanisms, Eur. J. Pharm. Sci. 130 (2019) 78–90. https://doi.org/10.1016/j.ejps.2019.01.019.

[34] J.J. García-Rodriguez, P.M. de la Torre-Iglesias, M.C. Vegas-Sánchez, S. Torrado-Durán, F. Bolás-Fernández, S. Torrado-Santiago, Changed crystallinity of mebendazole solid dispersion: Improved anthelmintic activity, Int. J. Pharm. 403 (2011) 23–28. https://doi.org/10.1016/J.IJPHARM.2010.10.002.

[35] D.R. Parakh, M.P. Patil, N.L. Dashputre, S.J. Kshirsagar, Development of self-microemulsifying drug delivery system of mebendazole by spray drying technology: Characterization, in vitro and in vivo evaluation, Dry. Technol. 34 (2016) 1023–1042. https://doi.org/10.1080/07373937.2015.1090447.

[36] V. Buchter, J. Priotti, D. Leonardi, M.C. Lamas, J. Keiser, Preparation, Physicochemical Characterization and In Vitro and In Vivo Activity Against Heligmosomoides polygyrus of Novel Oral Formulations of Albendazole and Mebendazole, J. Pharm. Sci. (2020) 1–8.

https://doi.org/10.1016/j.xphs.2020.02.002.

[37] G. Lemmens, J. Brouwers, J. Snoeys, P. Augustijns, T. Vanuytsel, Insight into the colonic disposition of celecoxib in humans, Eur. J. Pharm. Sci. 145 (2020) 105242. https://doi.org/10.1016/j.ejps.2020.105242.

[38] J.S. Choi, J. Bin Ahn, J.S. Park, Amorphous multi-system of celecoxib improves its anti-inflammatory activity in vitro and oral absorption in rats, Int. J. Pharm. 555 (2019) 135–145. https://doi.org/10.1016/j.ijpharm.2018.11.050.

[39] B.D. Monnery, V. V. Jerca, O. Sedlacek, B. Verbraeken, R. Cavill, R. Hoogenboom, Defined high molar mass poly(2-Oxazoline)s, Angew. Chemie - Int. Ed. 57 (2018) 15400–15404. https://doi.org/10.1002/anie.201807796.

[40] EMEA, ICH guideline Q3C (R6) on impurities: guideline for residual solvents, Int. Conf. Harmon. 68 (2016) 35.

[41] C. Luebbert, G. Sadowski, Moisture-induced phase separation and recrystallization in amorphous solid dispersions, Int. J. Pharm. 532 (2017) 635–646. https://doi.org/10.1016/j.ijpharm.2017.08.121.

[42] E.F.J. Rettler, H.M.L. Lambermont-Thijs, J.M. Kranenburg, R. Hoogenboom, M. V. Unger, H.W. Siesler, U.S. Schubert, Water uptake of poly(2-N-alkyl-2-oxazoline)s: influence of crystallinity and hydrogen-bonding on the mechanical properties, J. Mater. Chem. 21 (2011) 17331. https://doi.org/10.1039/c1jm12541a.

[43] C.S. Brazel, S.L. Rosen, Fundamental Principles of Polymeric Materials, Third Edition, Third, John Wiley & Sons, Inc., 2012.

[44] T. Xie, L.S. Taylor, Effect of Temperature and Moisture on the Physical Stability of Binary and Ternary Amorphous Solid Dispersions of Celecoxib, J. Pharm. Sci. 106 (2017) 100–110. https://doi.org/10.1016/j.xphs.2016.06.017.

[45] H. Chen, Y. Pui, C. Liu, Z. Chen, C.C. Su, M. Hageman, M. Hussain, R. Haskell, K. Stefanski, K. Foster, O. Gudmundsson, F. Qian, Moisture-Induced Amorphous Phase Separation of Amorphous Solid Dispersions: Molecular Mechanism, Microstructure, and Its Impact on Dissolution Performance, J. Pharm. Sci. 107 (2018) 317–326. https://doi.org/10.1016/j.xphs.2017.10.028.

[46] Y. Yani, P. Kanaujia, P.S. Chow, R.B.H. Tan, Effect of API-Polymer Miscibility and Interaction on the Stabilization of Amorphous Solid Dispersion: A Molecular Simulation Study, Ind. Eng. Chem. Res. 56 (2017) 12698–12707. https://doi.org/10.1021/acs.iecr.7b03187.

[47] J.A. Baird, L.S. Taylor, Evaluation of amorphous solid dispersion properties using thermal analysis techniques, Adv. Drug Deliv. Rev. 64 (2012) 396–421. https://doi.org/10.1016/j.addr.2011.07.009.

[48] F. Qian, J. Huang, M.A. Hussain, Drug–Polymer Solubility and Miscibility: Stability Consideration and Practical Challenges in Amorphous Solid Dispersion Development, J. Pharm. Sci. 99 (2010) 2941–2947. https://doi.org/10.1002/jps.22074.

[49] V.V. Jerca, F.A. Nicolescu, A. Baran, D.F. Anghel, D.S. Vasilescu, D.M. Vuluga, Synthesis and characterization of side-chain oxazoline–methyl methacrylate copolymers bearing azo-dye, React. Funct. Polym. 70 (2010) 827–835. https://doi.org/10.1016/j.reactfunctpolym.2010.07.018.

[50] H.A. Schneider, J. Rieger, E. Penzel, The glass transition temperature of random copolymers:

2. Extension of the Gordon-Taylor equation for asymmetric Tg vs composition curves, Polymer (Guildf). 38 (1997) 1323–1337. https://doi.org/10.1016/S0032-3861(96)00652-0.

[51] F. Qian, J. Huang, Q. Zhu, R. Haddadin, J. Gawel, R. Garmise, M. Hussain, Is a distinctive single Tg a reliable indicator for the homogeneity of amorphous solid dispersion?, Int. J. Pharm. 395 (2010) 232–235. https://doi.org/10.1016/j.ijpharm.2010.05.033.

[52] M. Gordon, J.S. Taylor, Ideal copolymers and the second-order transitions of synthetic rubbers. I. Noncrystalline copolymers, Rubber Chem. Technol. 26 (1953) 323–335. https://doi.org/10.5254/1.3539818.

[53] B.D. Anderson, Predicting Solubility / Miscibility in Amorphous Dispersions : It Is Time to Move Beyond Regular Solution Theories, J. Pharm. Sci. 107 (2017) 24–33. https://doi.org/10.1016/j.xphs.2017.09.030.

[54] T. Van Duong, G. Van den Mooter, The role of the carrier in the formulation of pharmaceutical solid dispersions. Part II: amorphous carriers, Expert Opin. Drug Deliv. 13 (2016) 1681–1694. https://doi.org/10.1080/17425247.2016.1198769.

[55] K. Löbmann, C. Strachan, H. Grohganz, T. Rades, O. Korhonen, R. Laitinen, Co-amorphous simvastatin and glipizide combinations show improved physical stability without evidence of intermolecular interactions, Eur. J. Pharm. Biopharm. 81 (2012) 159–169. https://doi.org/10.1016/j.ejpb.2012.02.004.

[56] M. Dirauf, A. Erlebach, C. Weber, S. Hoeppener, J.R. Buchheim, M. Sierka, U.S. Schubert, Block Copolymers Composed of PEtOx and Polyesteramides Based on Glycolic Acid, l-Valine, and l-Isoleucine, Macromolecules. 53 (2020) 3580–3590. https://doi.org/10.1021/acs.macromol.0c00282.

[57] F. Theil, J. Milsmann, S.O. Kyerematen, S. Anantharaman, J. Rg Rosenberg, H. Van Lishaut, Extraordinary Long-Term-Stability in Kinetically Stabilized Amorphous Solid Dispersions of Fenofibrate, Mol. Pharm. 14 (2017) 4636–4647. https://doi.org/10.1021/acs.molpharmaceut.7b00735.

[58] M.B. Rask, M.M. Knopp, N.E. Olesen, R. Holm, T. Rades, Influence of PVP/VA copolymer composition on drug-polymer solubility, Eur. J. Pharm. Sci. 85 (2016) 10–17. https://doi.org/10.1016/j.ejps.2016.01.026.

[59] R.J. Young, P.A. Lovell, Introduction to Polymers, Third Edition, Taylor & Francis, 2011.

[60] B.A. Wolf, Chain connectivity and conformational variability of polymers: Clues to an adequate thermodynamic description of their solutions, 2. Composition dependence of Flory-Huggins interaction parameters, Macromol. Chem. Phys. 204 (2003) 1381–1390. https://doi.org/10.1002/macp.200350002.

[61] E. Schoolaert, R. Merckx, J. Becelaere, M. Everaerts, J.F.R. Van Guyse, O. Sedlacek, B.G. De Geest, G. Van Den Mooter, D.R. D'Hooge, K. De Clerck, R. Hoogenboom, Immiscibility of Chemically Alike Amorphous Polymers: Phase Separation of Poly(2-ethyl-2-oxazoline) and Poly(2- n-propyl-2-oxazoline), Macromolecules. 53 (2020) 7590–7600. https://doi.org/10.1021/ACS.MACROMOL.0C00970/ASSET/IMAGES/LARGE/MA0C00970_0008.JPEG.

[62] D.. van Krevelen, K. te Nijenhuis, Properties of polymers. Their correlation with chemical structure; their numerical estimation and prediction from additive group contributions, 2009.

[63] C.M. Hansen, Hansen Solubility Parameters, CRC Press, Cambridge, 2007. https://doi.org/10.1201/9781420006834.

[64] K. Wlodarski, F. Zhang, T. Liu, W. Sawicki, T. Kipping, Synergistic Effect of Polyvinyl Alcohol and Copovidone in Itraconazole Amorphous Solid Dispersions, Pharm. Res. 35 (2018). https://doi.org/10.1007/s11095-017-2313-1.

[65] S. Zhang, T.W.Y. Lee, A.H.L. Chow, Thermodynamic and kinetic evaluation of the impact of polymer excipients on storage stability of amorphous itraconazole, Int. J. Pharm. 555 (2019) 394–403. https://doi.org/10.1016/j.ijpharm.2018.11.063.

[66] B. Kállai-Szabó, M. Sinka, B. Stiedl, I. Sebe, I. Antal, R. Zelkó, Tracking of the solubility enhancement and drug release stability of melt extrudates containing mebendazole, J. Drug Deliv. Sci. Technol. 24 (2014) 514–518. https://doi.org/10.1016/S1773-2247(14)50097-4.

[67] R. Ghanavati, A. Taheri, A. Homayouni, Anomalous dissolution behavior of celecoxib in PVP/Isomalt solid dispersions prepared using spray drier, Mater. Sci. Eng. C. 72 (2017) 501–511. https://doi.org/10.1016/J.MSEC.2016.11.042.

[68] S. Motallae, A. Taheri, A. Homayouni, Preparation and characterization of solid dispersions of celecoxib obtained by spray-drying ethanolic suspensions containing PVP-K30 or isomalt, J. Drug Deliv. Sci. Technol. 46 (2018) 188–196. https://doi.org/10.1016/j.jddst.2018.05.020.

[69] J.A. Lugtu-Pe, A. Ghaffari, K. Chen, A. Kane, X.Y. Wu, Development of controlled release amorphous solid dispersions (CRASD) using polyvinyl acetate-based release retarding materials: Effect of dosage form design, Eur. J. Pharm. Sci. 124 (2018) 319–327. https://doi.org/10.1016/j.ejps.2018.09.006.

[70] V.R. Kallakunta, S. Sarabu, S. Bandari, A. Batra, V. Bi, T. Durig, M.A. Repka, Stable amorphous solid dispersions of fenofibrate using hot melt extrusion technology: Effect of formulation and process parameters for a low glass transition temperature drug, J. Drug Deliv. Sci. Technol. 58 (2020) 101395. https://doi.org/10.1016/j.jddst.2019.101395.

[71] J. Bin Ahn, D.H. Kim, S.E. Lee, Y.C. Pyo, J.S. Park, Improvement of the dissolution rate and bioavailability of fenofibrate by the supercritical anti-solvent process, Int. J. Pharm. 564 (2019) 263–272. https://doi.org/10.1016/j.ijpharm.2019.04.051.

[72] S.C. Shen, W.K. Ng, J. Hu, K. Letchmanan, J. Ng, R.B.H. Tan, Solvent-free direct formulation of poorly-soluble drugs to amorphous solid dispersion via melt-absorption, Adv. Powder Technol. 28 (2017) 1316–1324. https://doi.org/10.1016/j.apt.2017.02.020.